*Inorg. Chem.* **2006**, *45*, 2038–2044


# Facile Controlled Synthesis of $MnO_2$ Nanostructures of Novel Shapes and Their Application in Batteries

**Fangyi Cheng, Jianzhi Zhao, Wene Song, Chunsheng Li, Hua Ma, Jun Chen,* and Panwen Shen**

*Institute of New Energy Material Chemistry, Nankai University, Tianjin 300071, P. R. China*

Received October 5, 2005

In this paper, $MnO_2$ nanomaterials of different crystallographic types and crystal morphologies have been selectively synthesized via a facile hydrothermal route and electrochemically investigated as the cathode active materials of primary and rechargeable batteries. $\beta$-$MnO_2$ nano/microstructures, including one-dimensional (1-D) nanowires, nanorods, and nanoneedles, as well as 2-D hexagramlike and dendritelike hierarchical forms, were obtained by simple hydrothermal decomposition of an $Mn(NO_3)_2$ solution under controlled reaction conditions. $\alpha$- and $\gamma$-$MnO_2$ nanowires and nanorods were also prepared on the basis of previous literature. The as-synthesized samples were characterized by instrumental analyses such as XRD, SEM, TEM, and HRTEM. Furthermore, the obtained 1-D $\alpha$- and $\gamma$-$MnO_2$ nanostructures were found to exhibit favorable discharge performance in both primary alkaline Zn–$MnO_2$ cells and rechargeable Li–$MnO_2$ cells, showing their potential applications in high-energy batteries.

## Introduction

Nanostructures have received steadily growing interest not only for their fundamental scientific significance but also for the many technological applications that derive from their peculiar and fascinating properties, superior to the corresponding bulk counterparts.[1,2] Recent studies have been focused on synthesizing 1-dimensional (1-D) nanostructures and constructing hierarchical structures or networks, which are expected to play an important role in fabricating the next generation of microelectronic and optoelectronic devices since they can function as both building units and interconnections.[3−9] For the purpose of property studies and future applications of nanoscale materials, it is doubtless that the primary objective should lie in developing various convenient synthetic strategies to obtain new nanostructures of novel shapes. Because of its easily controllable reaction condition and the relatively abundant reactant sources, the so-called soft chemical route, based on a solution process, might provide an attractive option for large-scale production of nanomaterials with special morphology. For example, numerous studies have been reported on the synthesis of peculiar materials by hydrothermal or solvothermal methods,[10−12] and in particular, large quantities of inorganic materials including metals, chalcogenides, and metal oxides/hydroxides are achieved in nanoscaled forms through such a route.[13−16]

As an important functional metal oxide, manganese dioxide is one of the most attractive inorganic materials because of its physical and chemical properties and wide applications in catalysis, ion exchange, molecular adsorption, biosensor, and particularly, energy storage.[17−23] It is well-

* To whom correspondence should be addressed. E-mail: chenabc@nankai.edu.cn.

(1) Nalwa, H. S. *Handbook of Nanostructured Materials and Nanotechnology*; Academic Press: New York, 2000.
(2) Burda, C.; Chen, X. B.; Narayanan, R.; El-Sayed, M. A. *Chem. Rev.* **2005**, *105*, 1025.
(3) Hu, J. T.; Odom, T. W.; Lieber, C. M. *Acc. Chem. Res.* **1999**, *32*, 435.
(4) Forster, P. M.; Cheetham, A. K. *Angew. Chem., Int. Ed.* **2002**, *41*, 457.
(5) Xia, Y. N.; Yang, P. D.; Sun, Y. G.; Wu, Y. Y.; Mayer, B.; Gates, B.; Yin, Y. D.; Kim, F.; Yan, H. Q. *Adv. Mater.* **2003**, *15*, 353.
(6) (a) Wang, X.; Zhuang, J.; Peng, Q.; Li, Y. D. *Nature* **2005**, *437*, 121. (b) Wang, J. W.; Wang, X.; Li, Y. D. *Inorg. Chem.* **2004**, *43*, 7552.
(7) Lao, J. Y.; Wen, J. G.; Ren, Z. F. *Nano Lett.* **2002**, *2*, 1287.
(8) Dick, K. A.; Deooert, K.; Larsson, M. W.; Martensson, T.; Seifert, W.; Wallenberg, L. R.; Samuelson, L. *Nat. Mater.* **2004**, *3*, 380.
(9) Wang, Z. L. *Adv. Mater.* **2003**, *15*, 432.
(10) Shahriari, D. Y.; Barnabè, A.; Mason, T. O.; Poeppelmeier, K. R. *Inorg. Chem.* **2001**, *40*, 5734.
(11) Feng, S. H.; Xu, R. R. *Acc. Chem. Res.* **2001**, *34*, 239.
(12) Walton, R. I. *Chem. Soc. Rev.* **2002**, *31*, 230.
(13) Wei, S.; Lu, J.; Yu, W.; Zhang, H.; Qian, Y. *Inorg. Chem.* **2005**, *44*, 3844.
(14) Qiu, L.; Wei, Y.; Pol, V. G.; Gedanken, A. *Inorg. Chem.* **2004**, *43*, 6061.
(15) Yu, J. C.; Xu, A.; Zhang, L.; Song, R.; Wu, L. *J. Phys. Chem. B* **2004**, 108, 64.
(16) Ding, Y.; Zhang, G.; Wu, H.; Hai, B.; Wang, L.; Qian, Y. *Chem. Mater.* **2001**, *13*, 435.
(17) (a) Chabre, Y.; Pannetier, J. *Prog. Solid State Chem.* **1995**, *23*, 1. (b) Thackeray, M. M. *Prog. Solid State Chem.* **1997**, *25*, 1.
(18) Espinal, L.; Suib, S. L.; Rusling, J. F. *J. Am. Chem. Soc.* **2004**, *126*, 7676.



10.1021/ic051715b CCC: $33.50 
Published on Web 02/02/2006

known that manganese dioxide can exist in different structural forms, α-, *β*-, *γ*-, and *λ*-types, etc., when the basic structure unit (namely, the [$MnO_6$] octahedron) is linked in different ways. Much effort has been directed toward the preparation of low-dimensional $MnO_2$ nanostructures with various polymorphs. For example, α-, *β*-, and *γ*-$MnO_2$ were prepared in different morphologies, such as rods, wires, tubes, etc., using hydrothermal techniques.[24−28] However, few reports have been focused on the formation of $MnO_2$ hierarchical architecture.[29] In addition, until now the investigation of the application of 1-D nanostructured manganese dioxide as electrode materials still remains limited,[30] although the shape and size of inorganic materials is generally believed to influence their properties and performances. In these regards, we report in this paper the synthesis of $MnO_2$ nanostructures with novel shapes and their application as cathode materials in batteries.

In our work, *β*-$MnO_2$ was synthesized by simply decomposing a $Mn(NO_3)_2$ solution under hydrothermal conditions. The formation of different morphologies, including one-dimensional (1-D) nanorods and nanowires as well as 2-D hierarchical nanostructures, was achieved by controlling the hydrothermal reaction parameters. This synthetic route requires no templates, catalysts, or organic reagents and therefore can be scaled up to produce novel-shaped $MnO_2$ nanocrystals without special postsynthesis treatment for purification. Furthermore, to investigate the electrode properties of nanostructured $MnO_2$, we also prepared α- and *γ*-$MnO_2$ nanowires/nanorods on the basis of the work reported by Li et al.[24] Electrochemical measurements showed that the as-synthesized α- and *γ*-$MnO_2$ nanostructures exhibit relatively good discharge performance as the cathode active materials in both the laboratory-made primary alkaline Zn−$MnO_2$ cells and rechargeable lithium-ion cells. The present results should foster the application of inexpensive and low-toxicity α- and *γ*-$MnO_2$ 1-D nanostructures in energy storage, and they should also provide a facile route for mass production of *β*-$MnO_2$ crystals with hierarchical nanostructures. This may also find potential application in other aspects of material science such as reinforcing composite materials or further modifying other nanoarchitectures.

## Experimental Section

**Synthesis.** All chemicals were of analytical grade and were used as purchased without further purification. $MnSO_4 \cdot H_2O$, $MnNO_3$ (50 wt % solution), $KMnO_4$, and $(NH_4)_2S_2O_8$ were all supplied by Tianjin Chemical Reagent Company (P. R. China). Deionized water was used throughout.

*β*-$MnO_2$ was prepared through hydrothermal treatment of a $Mn(NO_3)_2$ aqueous solution. A series of parallel experiments were carried out by altering the reaction parameters such as heating temperature, reactant concentration, and reaction time. In brief, the synthesis process could be described as follows: an $Mn(NO_3)_2$ solution (0.1−4.0 M) was loaded into a Teflon-lined stainless steel autoclave and heated at 160−180 °C for 3−72 h. The autoclave was allowed to cool to room temperature after the dwell time. Then, the powders obtained were collected and washed repeatedly with distilled water to remove any possible residual reactant. Finally, the $MnO_2$ precipitated was dried in air at 40 °C. In another experiment, nitric acid was added to the starting $Mn(NO_3)_2$ solution so that the influence of acid on the product morphology could be investigated. The details are available later in the text.

The synthesis of α- and *γ*-$MnO_2$ was carried out on the basis of the previous work of Li's group with little modification.[24] In a typical synthesis of α-$MnO_2$, 0.2 g of $MnSO_4 \cdot H_2O$ and 0.5 g of $KMnO_4$ were mixed in distilled water and magnetically stirred to form a homogeneous mixture, which was then transferred into a Teflon-lined stainless steel autoclave and heated at 140 °C for 12 h. For the preparation of *γ*-$MnO_2$, stoichiometric moles of $MnSO_4$ and $(NH_4)_2S_2O_8$ were well mixed and hydrothermally treated at 90 °C for 24 h. The product was collected, washed, and dried in a manner similar to that of *β*-$MnO_2$.

**Characterization.** The powder X-ray diffraction (XRD) pattern was measured on a Rigaku D/max 2500 X-ray diffractometer (Cu Kα radiation, $\lambda = 1.54178$ Å). Scanning electron microscope (SEM) and field-emission SEM (FE-SEM) images were taken using Philips XL-30 and JEOL JSM-6700F microscopes operated at the accelerating voltages of 20 kV and 10 kV, respectively. Transmission electron microscope (TEM) and high-resolution TEM (HRTEM) characterization was performed with a Philips Tecnai F20 (accelerating voltage = 200 kV) microscope. For the sake of convenience, all SEM and FE-SEM images are briefly called SEM images later.

**Electrochemical Measurement.** The as-synthesized $MnO_2$ powders were employed as cathode active materials for alkaline primary Zn−$MnO_2$ cells and rechargeable lithium-ion cells. The fabrication of the laboratory cells and the composition of the electrolytes and anode electrodes resembled that presented in our previous work.[30a,31] For the alkaline cells, the working electrodes were composed of 85 wt % active materials ($MnO_2$), 8 wt % conductive materials (carbon), and 7 wt % binding agent (poly(tetrafluoroethylene) (PTFE) in KOH aqueous solution. The positive electrodes of the Li−$MnO_2$ cells were made of 85 wt % $MnO_2$, 10 wt % acetylene black, and 5 wt % PTFE. Electrochemical performance was investigated using the Land battery measurement system (Wuhan, P. R. China) at the controlled temperature of 25 °C. All the laboratory-made Zn−$MnO_2$ cells were discharged to an end voltage of 0.8 V at a constant current rate of 40 mA $g^{-1}$,

(19) Chitrakar, R.; Kanoh, H.; Kim, Y. S.; Miyai, Y.; Ooi, K. *J. Solid State Chem.* **2001**, *160*, 69.
(20) Armstrong, A. R.; Bruce, P. G. *Nature* **1996**, *381*, 499.
(21) Ammundsen, B.; Paulsen, J. *Adv. Mater.* **2001**, *13*, 943.
(22) Winter, M.; Brodd, R. J. *Chem. Rev.* **2004**, *104*, 4245.
(23) Toupin, M.; Brousse, T.; Bélanger, D. *Chem. Mater.* **2002**, *14*, 3946.
(24) (a) Wang, X.; Li, Y. D. *Chem.—Eur. J.* **2003**, *9*, 300. (b) Wang, X.; Li, Y. D. *J. Am. Chem. Soc.* **2002**, *124*, 2880.
(25) Xiong, Y. J.; Xie, Y.; Li, Z. Q.; Wu, C. Z. *Chem.—Eur. J.* **2003**, *9*, 1645.
(26) Wei, M.; Konishi, Y.; Zhou, H.; Sugihara, H.; Arakawa, H. *Nanotechnology* **2005**, *16*, 245.
(27) Yuan, Z. Y.; Ren, T. Z.; Du, G. H.; Su, B. L. *Appl. Phys. A* **2005**, *80*, 743.
(28) Zheng, D.; Sun, S.; Fan, W.; Yu, H.; Fan, C.; Cao, G.; Yin, Z.; Song, X. *J. Phys. Chem. B* **2005**, *109*, 16439.
(29) (a) Yuan, J.; Li, W. N.; Gomez, S.; Suib, S. L. *J. Am. Chem. Soc.* **2005**, *127*, 14184. (b) Li, Z.; Ding, Y.; Xiong, Y.; Xie, Y. *Cryst. Growth Des.* **2005**, *5*, 1953. (c) Li, Z. Q.; Ding, Y.; Xiong, Y. J.; Yang, Q.; Xie, Y. *Chem. Commun.* **2005**, *7*, 918.
(30) (a) Cheng, F. Y.; Chen, J.; Gou, X. L.; Shen, P. W. *Adv. Mater.* **2005**, *17*, 2753. (b) Sugantha, M.; Ramakrishnan, P. A.; Hermann, A. M.; Warmsingh, C. P.; Ginley, D. S. *Int. J. Hydrogen Energy* **2003**, *28*, 597.
(31) (a) Li, X. X.; Cheng, F. Y.; Guo, B.; Chen, J. *J. Phys. Chem. B* **2005** *109*, 14017. (b) Chen, J.; Xu, L. N.; Li, W. Y. *Adv. Mater.* **2005**, *17*, 582.

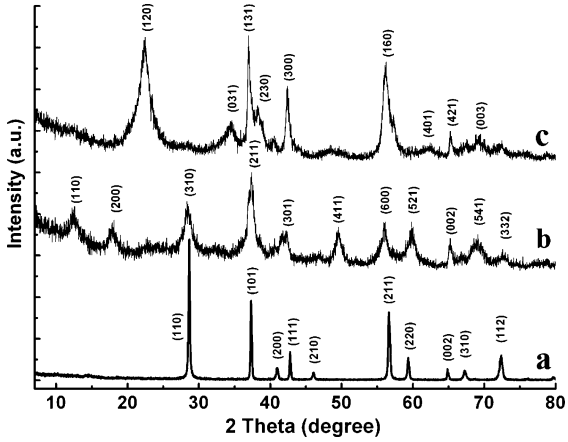


**Figure 1.** XRD patterns of the as-synthesized (a) $\beta$-, (b) $\alpha$-, and (c) $\gamma$-$MnO_2$ nanostructures.

while the Li−$MnO_2$ cells were cycled at the rate of 50 mA $g^{-1}$ in the voltage range of 3.8−1.5 V.

## Results and Discussion

**Composition of the Product.** The crystal phase of the samples was analyzed by powder X-ray diffraction. Figure 1 shows the XRD patterns of three representative products. All the diffraction peaks in Figure 1a can be indexed to tetragonal symmetry with a space group of *P*42/*mnm* (No.136). The lattice constants were calculated to be $a$ = 4.40 Å and $c$= 2.87 Å, which are in good agreement with the reported data for the pure phase of $\beta$-$MnO_2$ (ICDD-JCPDS No. 24-0735, $a$ = 4.399 Å and $c$ = 2.874 Å). Thus, the obtained $\beta$-$MnO_2$ products were of high purity and in good crystallinity. The XRD pattern in Figure 1b corresponds to $\alpha$-$MnO_2$ (ICDD-JCPDS Card No. 44-0141), and the pattern in Figure 1c confirms the formation of $\gamma$-$MnO_2$ (ICDD-JCPDS No. 14-0644). Meanwhile, the broadened diffraction peaks indicate that the crystalline sizes of the samples are small and that the crystallinity of $\alpha$- and $\gamma$-$MnO_2$ is not as good as that of $\beta$-$MnO_2$. The XRD analysis results presented here are similar to that reported in the literature,[24−27] in which $\alpha$- and $\gamma$-$MnO_2$, synthesized via a solution-based route, showed relatively poor crystallinity compared to that of $\beta$-$MnO_2$.

The chemical reaction involved in our present hydrothermal synthesis can be briefly described as

$$Mn(NO_3)_2 \rightarrow \beta\text{-}MnO_2 + 2NO_2\uparrow \text{ (a)}$$
$$4NO_2 + O_2 + 2H_2O \rightarrow 4HNO_3 \text{ (b)} \quad (1)$$

$$2KMnO_4 + 3MnSO_4 + 2H_2O \rightarrow 5\alpha\text{-}MnO_2 + K_2SO_4 + 2H_2SO_4 \quad (2)$$

$$MnSO_4 + (NH_4)_2S_2O_8 + 2H_2O \rightarrow \gamma\text{-}MnO_2 + (NH_4)_2SO_4 + 2H_2SO_4 \quad (3)$$

As can be seen in the above equations, the related reactions are quite simple: no catalyst or organic template is needed, all of the reactant is soluble in water, nad only the target product is in precipitate form. Hence it is easy to control the reaction system, and the rational synthesis of manganese dioxide with different morphologies and desired crystal forms becomes possible. Moreover, since all involved chemicals are of low cost and low toxicity and all procedures in the synthesis are facile to manipulate, large-scale production of nanostructured $MnO_2$ for practical application is possible.

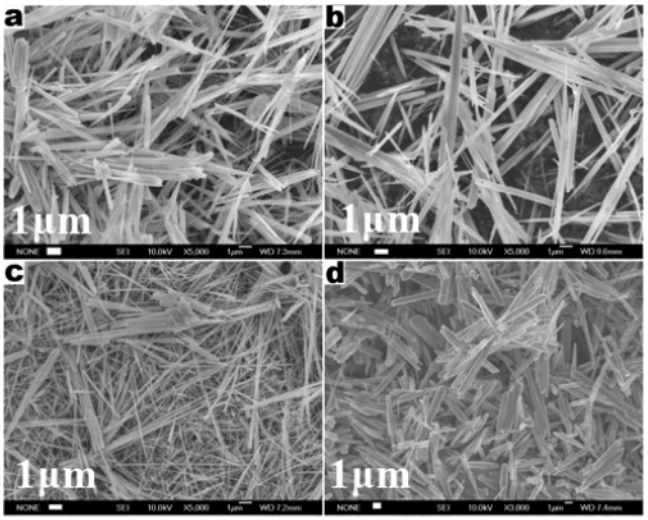


**Figure 2.** SEM images of the obtained one-dimensional $\beta$-$MnO_2$ materials at 170 °C and 6 h. Panels a, b, c, and d correspond to the samples synthesized from 0.2, 0.4, 0.6, and 0.8 M $Mn(NO_3)_2$ solutions, respectively.

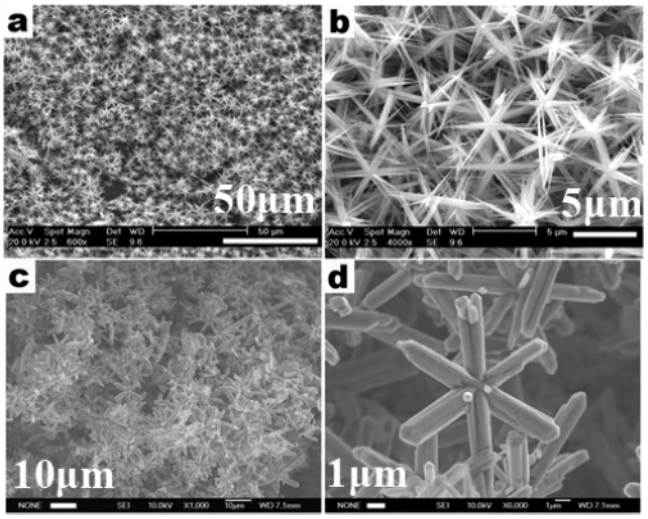


**Figure 3.** SEM images of the 2-D hexagonal starlike $\beta$-$MnO_2$ crytals synthesized from (a, b) 1.2 M and (c, d) 2.0 M $Mn(NO_3)_2$ solution.

**Morphology Characterization.** The morphologies of the $MnO_2$ powders obtained were examined by SEM, TEM, and HRTEM microscopy. To the best of our knowledge, few studies concerned the synthesis and characterization of $\beta$-$MnO_2$ hierarchical nanostructures, and there is no report on their preparation via simple hydrothermal treatment of a $Mn(NO_3)_2$ solution. So, in this part, we will at first emphasize the analysis of $\beta$-$MnO_2$ crystals of different shapes, and then we will briefly discuss the $\alpha$-$MnO_2$ and $\gamma$-$MnO_2$ nanostructures.

**1. $\beta$-$MnO_2$.** A series of experiments were carried out by varying the reaction parameters (i.e., reaction temperature, heating time, and reactant concentration). $\beta$-$MnO_2$ crystals with various shapes and sizes could be obtained under different conditions.

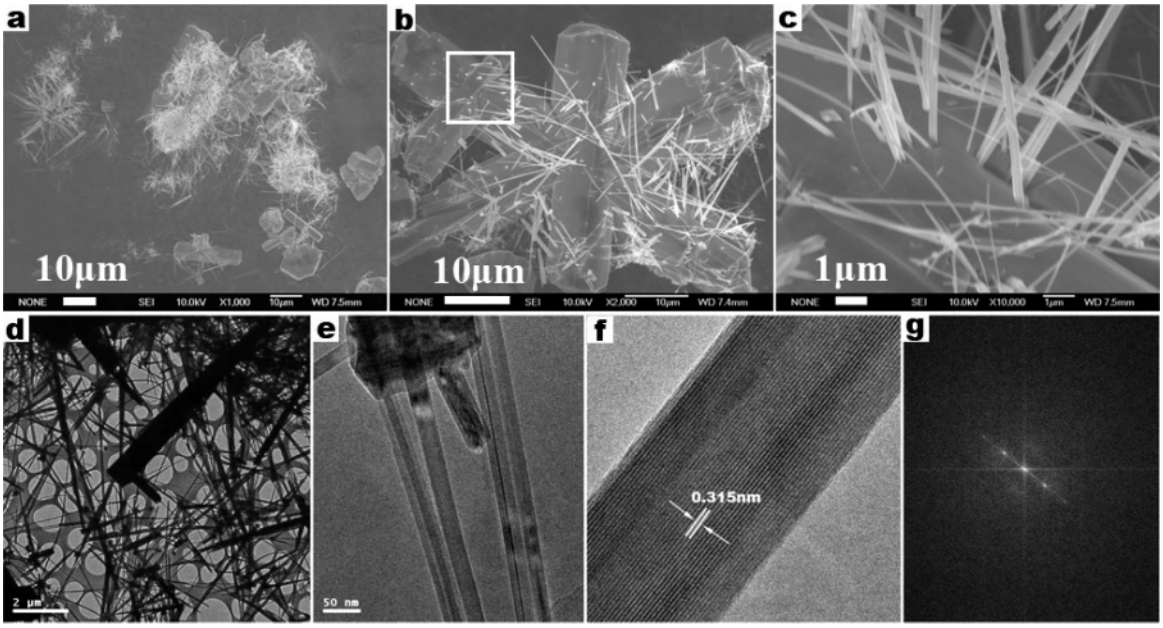


**Figure 4.** $\beta$-$MnO_2$ nanowires and microrods obtained from $Mn(NO_3)_2$ solution with the following reaction conditions: 1.0 M, 170 °C, 3 h. (a, b, c) SEM and (d, e) TEM images at different magnifications, (f) HRTEM image of a single nanowire, and (g) the corresponding FFT pattern taken from f.

Figure 2 shows the SEM images of the as-synthesized 1-D $\beta$-$MnO_2$ nano- and micromaterials. The four samples corresponding to Figure 2a, b, c, and d were obtained at 170 °C by controlling the starting concentration of the $Mn(NO_3)_2$ solution at 0.2, 0.4, 0.6, and 0.8 M, respectively. As can be seen in Figure 2a, both microrods and nanowires can be observed in the sample precipitated from the low-concentration solution. At a solution concentration of 0.4 M, the nanowires became larger in diameter (Figure 2b) and their morphology proportion to the whole product decreased. With a concentration of 0.8 M, all rods grew to the micrometer scale with much more uniform diameters and lengths (Figure 2d).

Figure 3 shows the SEM images of 2-D $\beta$-$MnO_2$ structures, which were obtained from hydrothermal treatment of a $Mn(NO_3)_2$ solution of higher concentration (>1.0 M). The low-magnification images in Figure 3a and c display large quantities of uniform hexagonal starlike or snowflake-shaped crystals. The higher magnification in Figure 3b and d clearly show the 6-fold structures, and in both cases, the six points of a "star" are roughly geometrically symmetric. The samples resulted from a 1.2 M $Mn(NO_3)_2$ solution have acicular tips in each crystal (Figure 3b), while flatter ends can be observed in the crystals obtained from a 2.0 M solution (Figure 3c). This difference may be the result of the different crystal growth velocities that occur in the two $Mn(NO_3)_2$ solutions.

Moreover, we have also found that when a medium starting concentration (1.0 M) was adopted, the morphology of the product obtained after a short dwell time was not uniform, as shown in Figure 4. From the low-magnification SEM image (Figure 4a), both nanowires and microrods can be clearly seen. A novel conjunct structure is shown in the higher-magnification SEM image (Figure 4b), in which the white square marks the cross-joint architecture. The further enlarged SEM image (Figure 4c) reveals that several nanowires stick out from the surface of the microrods. Details of these interesting structures are still under investigation because their growth mechanism is unclear. The TEM images in Figure 4d and e show the coexistence of nanowires and microrods. The nanowires are around 20 nm in diameters, and they are several micrometers in length. HRTEM analysis (Figure 4f) provides more detailed structural information about the nanowires, showing the apparent lattice fringes of the crystal. The interlayer distance is calculated to be 0.315 nm, which agrees well with the separation between the [110] planes of $\beta$-$MnO_2$. As can be seen in Figure 6g, the corresponding FFT pattern displays a spot line perpendicular to the lattice fringes of Figure 6f, further confirming the good crystallinity of $\beta$-$MnO_2$ and indicating that the length of the nanowire extends along the [110] direction.

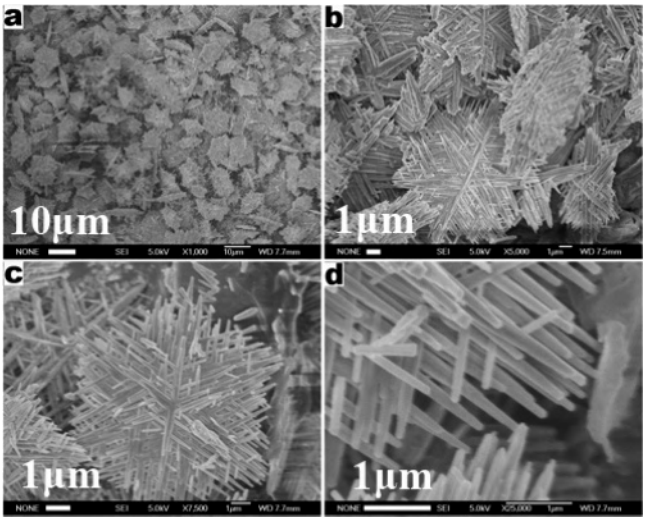


**Figure 5.** SEM images at different magnifications of the dendritelike hierarchical $\beta$-$MnO_2$ nanostructures synthesized from $Mn(NO_3)_2$ solution with the addition of nitric acid.

All above-mentioned $\beta$-$MnO_2$ products were synthesized directly via the hydrothermal decomposition of manganese

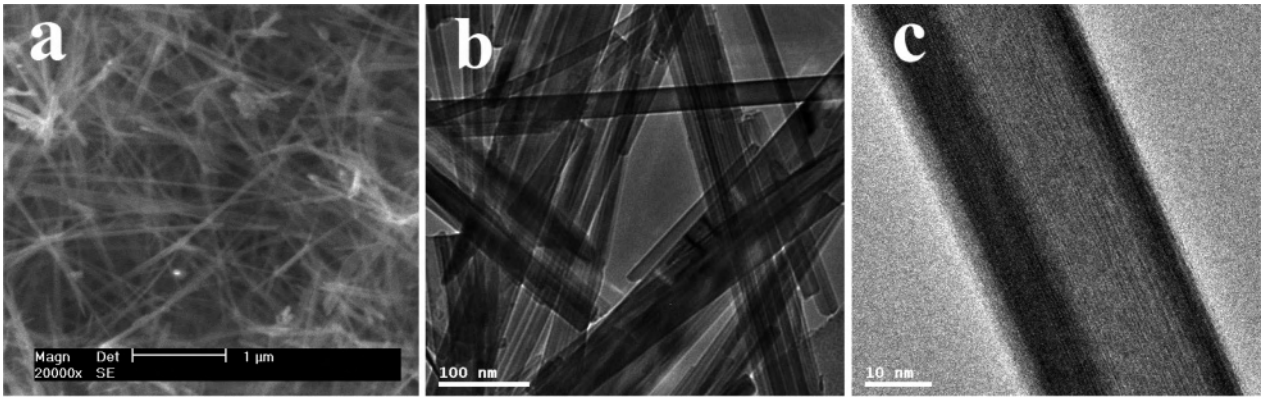


**Figure 6.** (a, b) Typical SEM and TEM images of the as-synthesized α-$MnO_2$ samples. (c) The corresponding HRTEM image of a single nanowire in b.

**Table 1.** Experimental Summary of the Synthesis of $\beta$-$MnO_2$ under Different Reaction Conditions

| | $T$ (°C) | dwell time (h) | $Mn(NO_3)_2$ (mol/L) | $HNO_3$ (mol/L) | morphology |
|---|---|---|---|---|---|
| 1 | 170 | 6 | 0.2−0.8 | 0 | nanowire and nanorod |
| 2 | 170 | 3 | 1.0 | 0 | nanowire and microrod |
| 3 | 170 | 12 | 1.2 | 0 | hexagonal starlike crystal (with acicular ends) |
| 4 | 170 | 12 | 2.0 | 0 | snowflake-shaped crystal (with cylindrical ends) |
| 5 | 170 | 3 | 1.0 | 0.12 | dendrite hierarchical structure |
| 6 | 170 | 72 | 1.0 | 1.0 | no visible precipitate |
| 7 | 180 | 24 | 2.0−4.0 | 0 | irregular microrod/particle |
| 8 | 160 | 3−24 | 1.0 | 0 | no visible precipitate |

nitrate solutions without any additional reagents. The pH is believed to have a large impact on the crystal growth of inorganic materials, and thus it influences the morphology of product.[32] Therefore, we added different amounts of acid to the starting $Mn(NO_3)_2$ solution and found that $\beta$-$MnO_2$ crystals of new shapes were obtained. Figure 5 shows the SEM images of the as-synthesized hierarchical nanostructures resulting from a 1.0 M $Mn(NO_3)_2$ solution with the addition of 0.12 M $HNO_3$. Large quantities of hexagon crystals can be seen in the panoramic SEM image (Figure 5a); the higher-magnification images (Figure 5b and c) clearly demonstrate the dendritic hierarchical structures, each of which consists of a core nanorod and several secondary nanorods that grow along the trunk rod in parallel. The further magnified image in Figure 5d shows that the nanorods of the hierarchical structures are straight and have smooth surfaces.

Table 1 summarizes the experimental result of the synthesis of $\beta$-$MnO_2$. The concentration of the starting material and the dwell time of the reaction are influential on the final morphology of product. Low reactant concentration and short duration time favors the formation of 1-D nanostructures (Figure 2) because of the anisotropic growth habits of the $MnO_2$ crystal, whereas a more concentrated $Mn(NO_3)_2$ solution tends to result in 2-D structures with larger crystals (Figure 3). Reaction temperature also has some influence on the product. At a heating temperature of 160 °C, no visible solid could be obtained in our synthesis. Thus, enough energy should be provided to the reaction system to allow the decomposition of $Mn(NO_3)_2$. At an elevated temperature of 180 °C, the crystal growth of $MnO_2$ was accelerated, leading to the formation of irregular microrods and microparticles (see Supporting Information Figure S1a). When nitric acid is added to the starting solution, hierarchical nanostructures can be formed (Figure 5) because of the epitaxial growth of 1-D $MnO_2$ nanorods from a common source. However, the addition of too much acid (pH = 0) would restrict the decomposition of $Mn(NO_3)_2$ because nitric acid is a result of the reaction (see eq 1). When the concentration of nitric acid in the initial solution exceeded 1.0 M, no $MnO_2$ precipitated even after a long reaction time of 72 h. Moreover, it should be noted that in some cases, we observed epitaxial growth and self-assembly of nanorods, which led to irregularly shaped $MnO_2$ crystals (Figure S1b−d).

**2. α-$MnO_2$ and γ-$MnO_2$.** The main purpose of synthesizing α- and γ-$MnO_2$ nanomaterials is, from a point view of concerning the emerging problem of power resources, to evaluate their performances in batteries, which is important for the utilization of inexpensive $MnO_2$ materials but has not gained much attention. The synthesis of α-$MnO_2$ and γ-$MnO_2$ was performed according to the previous work with little modification.[24] However, some of the morphology observations are somewhat different, which may be caused by the slightly altered specific experimental conditions. Figure 6a and b shows the representative SEM and TEM images of the obtained α-$MnO_2$ samples, respectively. Dispersive nanowires can be observed throughout the samples. Most of the wires are several micrometers in length and tens of nanometers in width, with a large aspect ratio. A HRTEM image (Figure 6c) of a single nanowire indicates the polycrystalline nature of the as-synthesized α-$MnO_2$, in agreement with the above XRD analysis. Figure 7a shows a typical SEM image of the as-prepared γ-$MnO_2$ sample, revealing high-yield growth of nanorods with lengths up to several micrometers. As can be seen in the low-magnification TEM image (Figure 7b), the synthesized rods are not uniform in diameter (20−100 nm). A HRTEM image (Figure 7c) of an individual nanorod demonstrates that the γ-$MnO_2$ obtained is of polycrystalline character and that the center of the rod exhibits better crystallinity than the outer part. We expect that the amorphous surface of γ-$MnO_2$ nanorods might provide more active sites for electrochemical reaction which

(32) (a) Kijima, N.; Yasuda, H.; Sato, T.; Yoshimura, Y. *J. Solid State Chem.* **2001**, *159*, 94. (b) Xiao, T. D.; Strutt, P. R.; Benaissa, M.; Chen, H.; Kear, B. H. *Nanostruct. Mater.* **1998**, *10*, 1051.

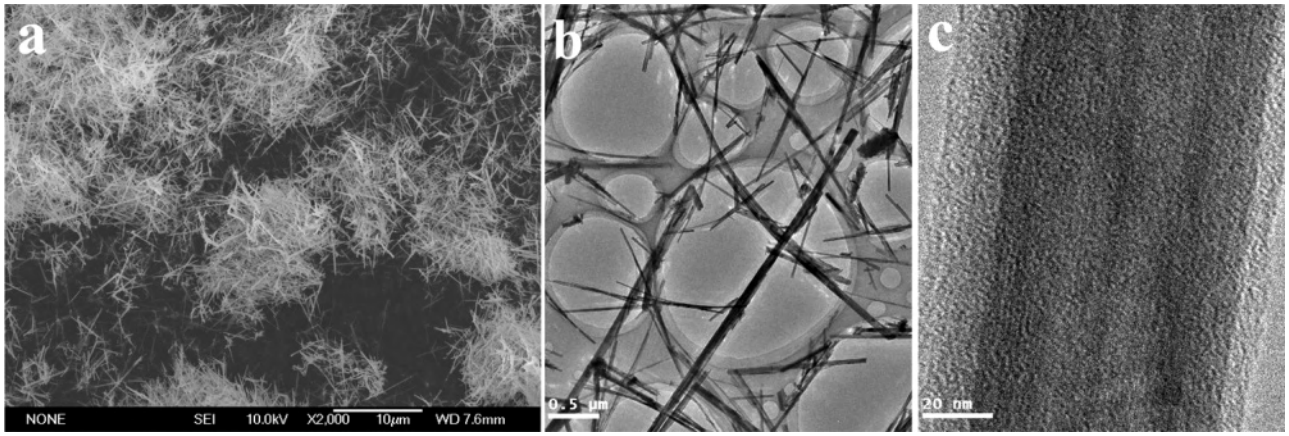


**Figure 7.** (a, b) Typical SEM and TEM images of the as-synthesized $\gamma$-$MnO_2$ nanorods. (c) HRTEM image of an individual nanorod.

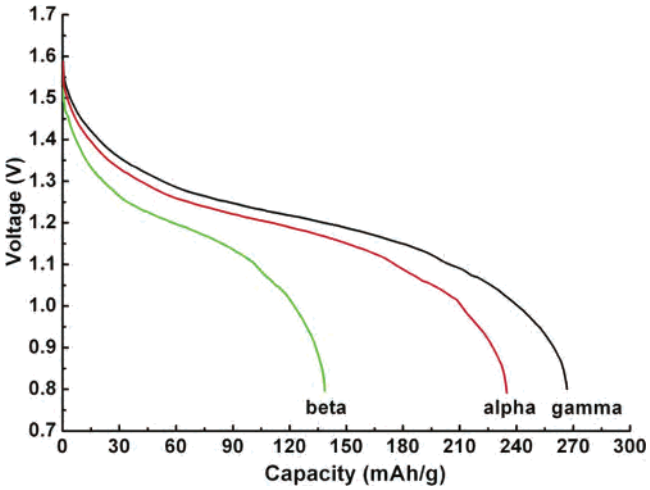


**Figure 8.** Discharge performance of the as-synthesized α-, $\beta$-, and $\gamma$-$MnO_2$ nanostructures in the laboratory-made alkaline Zn-$MnO_2$ cells (discharge condition: 40 mA $g^{-1}$, 25 °C).

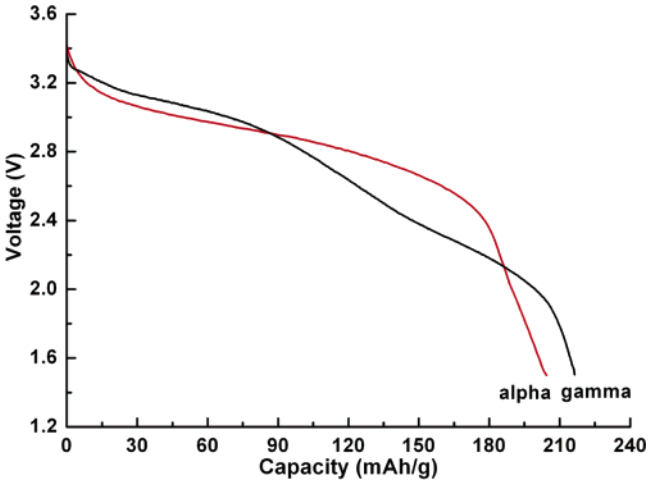


**Figure 9.** First discharge curves of the as-obtained α- and $\gamma$-$MnO_2$ nanostructures in the laboratory Li−$MnO_2$ cells. The discharge rate is 50 mA $g^{-1}$, and the temperature is set at 25 °C.

results in its better electrode performance, as will be discussed later.

**Application Studies.** Although the synthesis of $MnO_2$ 1-D nanomaterials with a desired crystal phase is often researched, the use of them in batteries and further comparison of their performance are rarely reported. So here we investigate the electrode properties of the as-synthesized α-, $\beta$-, and $\gamma$-$MnO_2$ nanostructures in alkaline primary Zn−$MnO_2$ cells and rechargeable Li−$MnO_2$ cells.

Figure 8 displays the discharge curves of the obtained α-, $\beta$-, and $\gamma$-$MnO_2$ 1-D nanostructures in laboratory-made alkaline Zn−$MnO_2$ cells to an end voltage of 0.8 V. It is obvious that α- and $\gamma$-$MnO_2$ nanowires/nanorods exhibit good discharge performance, both of which display sloping curves with an open-circuit potential of about 1.6 V and an average voltage of approximately 1.2 V. In addition, the synthesized α-$MnO_2$ nanowires deliver a discharge capacity of 235 mA h $g^{-1}$, while the prepared $\gamma$-$MnO_2$ nanorods exhibit a higher capacity of 267 mA h $g^{-1}$. In contrast, the initial voltage of $\beta$-$MnO_2$ nanostructures is lower, and their capacity is much smaller. Furthermore, we also evaluated the performance of $\gamma$-$MnO_2$ commercial powders usually used in batteries (see SEM images in Figure S2). As a comparison, the commercial $\gamma$-$MnO_2$ powders can merely deliver a discharge capacity of about 210 mA h $g^{-1}$, although they show a similar discharge curve to that of the $\gamma$-$MnO_2$ nanostructures (SI Figure S3). It's well-known that $\gamma$-$MnO_2$ exhibits better electrochemical performance than α- and $\beta$-$MnO_2$ in batteries.[17] However, the discharge capacity of the obtained α-$MnO_2$ nanowires in our work is even higher than that of the $\gamma$-$MnO_2$ commercial powders. Hence, the as-synthesized 1-D nanostructured α- and $\gamma$-$MnO_2$ show enhanced discharge performance in alkaline cells compared to their counterparts composed of the materials normally used in batteries.

Figures 9 and 10 show the first discharge behaviors and cycling performances of the laboratory-made Li−$MnO_2$ cells that are constructed of the as-synthesized α- and $\gamma$-$MnO_2$ nanostructures. The first discharge curve of the α-$MnO_2$ nanostructures shows a flat plateau in the voltage range between 3.0 and 2.5 V, and the discharge capacity reaches 204.4 mA h $g^{-1}$ to an end voltage of 1.5 V. This value is comparable to the reported data of α-$MnO_2$ nanofibers and is much higher than that of the related bulk materials.[30b] Recently, Kijima et al. reported a first discharge capacity of 230 mA h $g^{-1}$ at a lower current rate of 10 mA $g^{-1}$ for their prepared α-$MnO_2$ specimen, which showed reversibility during $Li^+$ insertion/extraction reactions but with a steady

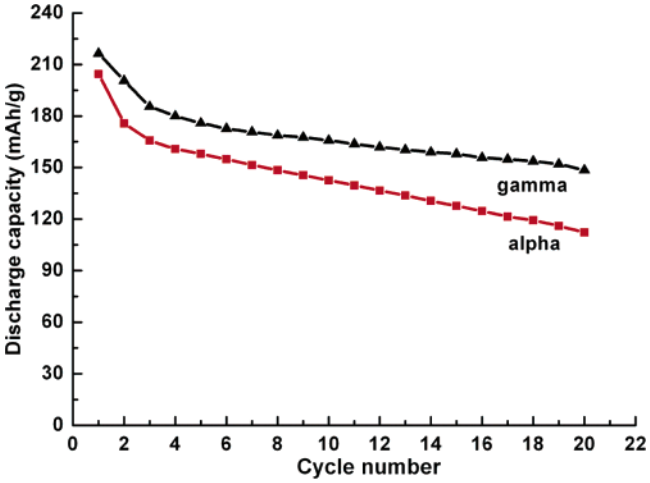


**Figure 10.** Discharge capacities of the as-prepared α- and $\gamma$-$MnO_2$ nanostructures over the first 20 cycles.

loss of capacity on cycling.[33] In our work, the synthesized α-$MnO_2$ nanowires also exhibited a continuous capacity drop during the repeated charge/discharge process. However, after cycling at the current rate of 50 mA $g^{-1}$ for 20 cycles, the nanowires still retained an acceptable capacity of 112 mA h $g^{-1}$. For $\gamma$-$MnO_2$ nanorods, the open-circuit potential was 3.43 V, and the discharge capacity exceeded 210 mA h $g^{-1}$, indicating that a desirable amount of lithium inserted (in $Li_x$-$MnO_2$, $x \approx 0.70$). After a significant capacity drop in the first three cycles, the $\gamma$-$MnO_2$ nanostructures presented favorable cycling capability during the subsequent charge/discharge. From the fourth to the twentieth cycle, the average capacity loss was less than 2 mA h $g^{-1}$ per cycle. As a comparison, the $\gamma$-$MnO_2$ commercial powders delivered a first discharge capacity of 180 mA h $g^{-1}$ and retained only 55% of the initial capacity after cycling for 20 cycles (Figures S4 and S5).

The improved electrode properties of the α- and $\gamma$-$MnO_2$ nanostructures may be the result of the 1-D morphology, which minimizes the distance over which protons or $Li^+$ must diffuse during the electrode process[31,34] in Zn−$MnO_2$ or Li−$MnO_2$ cells. Moreover, compared to the bulk counterparts, the, relatively, poorly crystalline $MnO_2$ nanomaterials might possess high surface areas[30b] and provide more active sites for the contact between electrode material and electrolyte. Accordingly, we believe that 1-D $MnO_2$ nanostructures are beneficial to faster diffusion kinetics and decreased electrode polarization. Further studies are underway on nanostructured $MnO_2$ using more analysis techniques, such as cyclic voltammograms (CV) and electrochemical impedance spectroscopy (EIS).

The electrochemical performance of $\beta$-$MnO_2$ nanostructures in Li−$MnO_2$ cells was still undesirable, since the first discharge capacity was less than 80 mA h $g^{-1}$ and the capacity quickly fell below 20 mA h $g^{-1}$ within five cycles (Figures S6 and S7). This result is consistent with earlier reports, in which the highly crystalline $\beta$-$MnO_2$ was found to show poor capacity and cycling capability.[17b] However, Tang et al. demonstrated that a $\beta$-$MnO_2$ nanocrystal/acetylene black composite is an excellent electrochemical lithium insertion material.[35] Perner's group also reported a new α/$\beta$-$MnO_2$ composite cathode material which showed superior performance for lithium cells.[36] Thus, by modifying or combining it with other components, the as-prepared $\beta$-$MnO_2$ nanostructures are likewise possible to find application as electrode materials in rechargeable batteries.

## Conclusions

In summary, we have demonstrated the synthesis and application of $MnO_2$ nanomaterials with different crystallographic forms and morphologies. α-, $\beta$-, and $\gamma$-$MnO_2$ nanostructures can be selectively prepared in high yields through a facile solution route. $\beta$-$MnO_2$ crystals with various shapes, including 1-D nanowires/nanorods, 2-D hexagonal starlike structures, and dendritelike hierarchical nanostructures, were synthesized via the simple hydrothermal decomposition of a $Mn(NO_3)_2$ aqueous solution. Electrochemical investigations indicate that the α- and $\gamma$-$MnO_2$ 1-D nanostructures obtained exhibit favorable performance as cathode active materials in both laboratory-made alkaline primary Zn−$MnO_2$ cells and rechargeable Li−$MnO_2$ cells. The present study should promote the use of $MnO_2$ 1-D nanomaterials to construct high-power batteries. Furthermore, these nanocrystals with novel morphologies may also find potential applications in sensors, catalysis, microelectronic devices, etc.

**Acknowledgment.** This work was supported by the foundation of NSFC (20325102 and 90406001), 973 Program (2005CB623607) and Ministry of Education (104055).

**Supporting Information Available:** Figures showing SEM images of $\beta$-$MnO_2$ crystals of irregular shapes and $\gamma$-$MnO_2$ commercial powders, discharge curves of the a laboratory-made Zn−$MnO_2$ cell with commercial $\gamma$-$MnO_2$ powders, a laboratory-made Li−$MnO_2$ cell made with commercial $\gamma$-$MnO_2$ powders, and a laboratory-made Li−$MnO_2$ cell with as-synthesized $\beta$-$MnO_2$ nanorods/wires, evolution of the discharge capacity of the commercial $\gamma$-$MnO_2$ powders over the first 20 cycles, and the cycling capacity of a laboratory-made Li−$MnO_2$ cell with as-obtained $\beta$-$MnO_2$ nanorods/wires. This material is available free of charge via the Internet at http://pubs.acs.org.

IC051715B

(33) Kijima, N.; Takahashi, Y.; Akimoto, J.; Awaka, J. *J. Solid State Chem.* **2005**, *178*, 2741.
(34) (a) Bueno, P. R.; Leite, E. R. *J. Phys. Chem. B* **2003**, *107*, 8868. (b) Nishizawa, M.; Mukai, K.; Kuwabata, S.; Martin, C. R.; Yoneyama, H. *J. Electrochem. Soc.* **1997**, *144*, 1923.
(35) Tang, W.; Yang, X.; Liu, Z.; Ooi, K. *J. Mater. Chem.* **2003**, *13*, 2989.
(36) Perner, A.; Holf, K.; Ilic, D.; Wohlfahrt-Mehrens, M. *Eur. J. Inorg. Chem.* **2002**, *5*, 1108.